Assisted-pinched transport of heavy-ion beams in a fusion chamber

D. R. Welch,[a] T. C. Genoni, D. V. Rose, B. V. Oliver, and R. E. Clark
Mission Research Corporation, 5001 Indian School Road NE, Albuquerque, New Mexico 87110

C. L. Olson
Sandia National Laboratories, P.O. Box 5800, Albuquerque, New Mexico 87185

S. S. Yu
Lawrence Berkeley National Laboratory, 1 Cyclotron Road, Mail Stop 47-112, Berkeley, California 94720

(Received 3 February 2003; accepted 5 March 2003)

In heavy-ion inertial confinement fusion, ion beams are transported several meters through the reactor chamber to the target. This standoff distance mitigates damage to the final focus magnets and chamber walls from the target explosion. A promising transport scheme makes use of a preformed discharge channel to confine and guide the beams. In this assisted-pinched transport scheme, many individual beams are merged into two high-current beams for two-sided illumination of the fusion target. The beams are combined and focused outside the chamber before propagating at small radius in the discharge channel to the target. A large beam divergence can be contained by the strong magnetic field resulting from the roughly 50-kA discharge current. Using a hybrid particle-in-cell simulation code, we examine the dynamics of heavy-ion inertial confinement fusion driver-scale beams in this transport mode. Results from detailed two-dimensional simulations of assisted-pinched transport in roughly 1-Torr Xe suggest that the Xe plasma becomes sufficiently conductive to limit self-field effects and achieve good transport efficiency. Coupling to a published target design is calculated. In addition, results from a semianalytic theory for resistive hose growth are presented that explain three-dimensional simulation results. © *2003 American Institute of Physics.* [DOI: 10.1063/1.1570421]

I. INTRODUCTION

Heavy-ion inertial confinement fusion (HIF) requires the focusing and transport of ion beams over several meters through the chamber to the target.[1] A sizable transport distance prevents damage to the final focus section of the accelerator and chamber wall from the target explosion.[2] To reduce the cost of the accelerator driver, current HIF designs include lower energy and higher current ion beams. These larger-perveance beams require a higher degree of ion charge and current neutralization in the chamber. Ballistic transport (mainline transport mode for the U.S. HIF program) uses a final focusing lens just outside the chamber to focus each beam onto the target and a supply of electrons to provide neutralization (neutralized-ballistic transport, or NBT).[3] Assisted-pinched transport (APT) uses a preformed channel created in a gas (1–10 Torr) by a laser and a z-discharge electrical circuit to create a frozen magnetic field before the ion beam is injected.[4–6] Self-pinched transport (SPT) uses the ion beam to break down a low-pressure gas (1–100 mTorr),[7–10] and the net self-magnetic field confines the beam. A recent review of these leading candidate schemes can be found by Olson.[11] These transport schemes impact the design, not only of the accelerator, but also of the fusion target.

NBT, the current U.S. HIF program baseline, requires $>90\%$ charge neutralization.[12] Plasma generators are required to supply neutralizing electrons near the region of injection into the chamber.[13] Some neutralization is also provided by ionization of the background gas (~ 1 mTorr) and by photoionization from early-time target radiation.[14] This option is attractive for the short transport lengths (roughly 3 m) envisioned for thick liquid-wall chambers[13] because the deleterious effects of space charge grow with transport distance. Pinched modes are possible for all chamber scenarios including wetted-wall and dry-wall that typically require larger chambers, and, hence, longer transport lengths of order 4–6 m. Both pinch modes are attractive because the chamber entrance holes are small, and because these modes accept beams with less stringent requirements on beam emittance and longitudinal energy spread.

Channel transport has already been demonstrated with high-current light ion beams in wall-stabilized discharges.[2,5,6,15] At the Naval Research Laboratory, 50–500 kA of 1-MeV protons have been efficiently transported over distances of 2–5 m.[15] Transport in freestanding laser-generated discharges was pioneered at Sandia National Laboratories.[5,16] Recently, channel experiments at Lawrence Berkeley National Laboratory have demonstrated stable channels with currents of 55 kA and a 4-mm radius.[17] Low-current heavy-ion beams have been successfully transported in these discharges.[18] The present HIF channel transport scenario uses two clusters of beams.[19] For each cluster, several beams are combined in an adiabatic lens (a tapered discharge channel[20–22]) and then injected into a single main z-discharge channel. Initial simulations of APT including self-field

[a]Electronic mail: drwelch@mrcabq.com

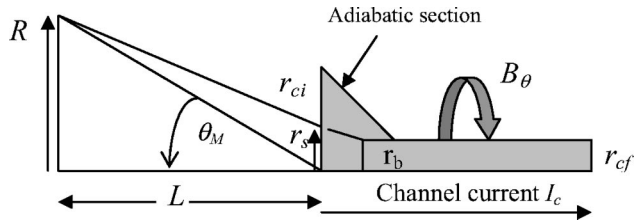

FIG. 1. A schematic of the APT system is sketched. After the final focus magnet, many beams of radius R are transported a distance L, captured and combined in the adiabatic discharge lens, compressed, and transported to the target.

effects[23] have shown the importance of including the resistive decay of plasma currents.

In this paper, we focus on the APT scheme pertaining to a thick-liquid wall chamber (radius of 3 m). We make use of the hybrid simulation code IPROP (Ref. 24) that includes modeling of the gas breakdown for 1-Torr ambient Xe gas pressure. Here, detailed 2D simulations of full driver pulses and coupling to a target are shown. The paper is organized as follows. A simple theory of the APT focusing system is derived in Sec. II. Detailed 2D calculations of target coupling are discussed in Sec. III. A semianalytic description of the resistive hose instability is presented with results in Sec. IV. Our conclusions follow in Sec. V.

II. BASIC ASSISTED-PINCHED TRANSPORT THEORY

The basic scheme for the transport of HIF beams in discharge plasma channels is shown in Fig. 1. The discharge is created in two stages. Guided by laser ionization, an electrical prepulse forms a reduced density channel in the ambient 5-Torr Xe gas. Then, a main pulse produces the 50-kA discharge. Ion beams are combined into two channels that terminate at opposing sides of the fusion target. Return current channels are created at right angles to the beam carrying channels for symmetry considerations. The basic concept behind pinched transport modes, including APT and SPT, is that the outward force caused by the beam divergence is contained by the $\mathbf{u}\times\mathbf{B}$ Lorentz force. For identical Bennett beam and net current profiles, the matched divergence in a discharge or self-field channel of total net current $I_{\rm net}$ (sum of beam and all plasma currents, including the discharge current if any) is given by the well-known Bennett pinch condition,

$$I_{\rm net}=\theta^2 I_A, \tag{1}$$

where $I_A=mc^3/Ze\gamma\beta_z$ is the ion Alfvén current. For relevant HIF parameters, $I_{\rm net}$ of 10–50 kA is sufficient. In the APT scenario,[4] many beams are captured at 1-cm radius in a tapered discharge channel that combines and compresses the beams to roughly 0.5-cm radius. Simulations, accounting for the magnetic fields of the 50-kA discharge current (I_d) but neglecting beam self fields, have shown excellent capture, adiabatic focusing, and transport of a HIF beam.[25] Initial simulations of APT transport including self fields have shown reduced, but adequate, efficiency.[23] If we ignore self fields and assume single particle trajectories, the beam radius can be computed from a simple energy argument relating the Lorentz potential to the incoming transverse energy of the beam and by making use of an adiabatic invariant. If we assume a uniform discharge current density, the potential (normalized by the electron rest mass energy) as a function of radius r is given by

$$A=\frac{Ze^2 I_c\beta_z}{mc^2}\left(\frac{r}{r_c}\right)^2, \tag{2}$$

where r_c is the channel radius and I_c is the channel current. Now an ion entering the channel with initial radius r_i and with divergence θ_i will reach a maximum radial excursion given by

$$r_{i0}=\left(r_i^2+\frac{1}{2}\frac{I_A}{I_c}\theta_i^2 r_{ci}^2\right)^{1/2}. \tag{3}$$

As the adiabatic channel radius decreases from its initial radius r_{ci} to its final radius r_{cf}, the maximum ion excursion, or Larmor radius, can be determined, assuming the magnetic flux encircled by the ion orbit is an adiabatic invariant for a slowly varying radius. For a linearly focused beam with outer radius r_s and focusing angle θ_m, the rms beam radius at equilibrium is given by

$$r_b=\frac{1}{2}\left[\frac{r_{cf}}{r_{ci}}\right]^{2/3}\sqrt{2r_s^2+\frac{I_A}{I_c}\theta_m^2 r_{ci}^2}. \tag{4}$$

The equation shows that the initial Larmor radii of the ions can be adiabatically compressed by the ratio of final-to-initial channel radius to the 2/3 power. The required current still scales as the Bennett pinch condition. One can easily find the optimal initial channel radius if we assume $r_b=r_{cf}$ and minimize the discharge current with respect to the r_{ci}. We find that the optimized $r_{ci}=3^{3/4}(r_s^3 r_{cf})^{1/2}$. Using the above results, for nominal parameters under consideration, $r_s=1$ cm, $r_{cf}=r_b=0.5$ cm, $\theta_m=0.03$ rad, the required discharge current from the above equation is 42 kA with $r_{ci}=3.2$ cm.

A key assumption made in the above theory is that self fields can be neglected, i.e., the plasma conductivity is infinite. In this limit, the discharge magnetic field remains constant and beam ions follow single-particle trajectories. For finite conductivity, σ, the growth in time t of net current $I_{\rm net}$ rises linearly from 0 to the beam current I_b in time $\tau_m=\pi\sigma r_b^2/c^2$ (the magnetic diffusion time). A rise in $I_{\rm net}$ comparable to discharge current I_d can lead to a nonlinear nonuniform focusing force and instability. For $I_b=6$ MA, to keep the rise in $I_{\rm net}\ll I_d$ for an 8-ns pulse, $\tau_m\gg 1\ \mu$s. For a 0.5-cm beam radius, this requires $\sigma\gg 10^{15}\ {\rm s}^{-1}$. This requirement on conductivity sets a lower limit on the plasma electron temperature of roughly $20Z-100Z$ eV.

III. 2D IPROP SIMULATIONS OF ASSISTED-PINCHED TRANSPORT

In this section, we present 2D simulations including the effects of beam self fields and gas interaction using the IPROP code.[23,24] These simulations are electromagnetic and make use of a tensor conductivity model to describe the plasma electron current. The HIF ion beams envisioned for APT are highly stripped ($Z>60$) in the Xe gas and reach MA electrical currents. Beam ionization is so intense that the weak-

plasma assumption is no longer valid. Modifications to the code involved simplified models of the discharge channel initial conditions, collisional heating and stripping of the gas by the beam. The results show the effect of self fields that contribute to degraded beam transport through inductive erosion; emittance growth and hose instability can be tolerated due to the production of a highly conductive plasma. IPROP uses a two-fluid treatment for the plasma ions and electrons. The plasma electrons have temperature T_e and momentum transfer frequency ν_m. The Ohm's law for plasma electron current used in the electromagnetic field solver is $\mathbf{J}_e = \sigma(\nabla p_e/n_e - \mathbf{u}_i\nu_m + \mathbf{E} + \mathbf{u}\times\mathbf{B})$, where $p_e(n_eT_e)$, n_e, and $\mathbf{u}_i$ are the electron pressure, electron density, and plasma ion velocity, respectively. The plasma ions are treated with Lagrangian fluid equations. The energy equation includes only the self-work term and the electron-ion thermalization term characterized by the usual equilibration time τ_{ie},

$$\frac{3}{2}n_i\frac{dT_i}{dt} = -p_i\nabla\cdot u_i + \frac{3n_em_e}{n_im_i\tau_{ie}}(T_e - T_i), \tag{5}$$

where n_i, T_i, and p_i are the plasma ion density, temperature, and pressure (n_iT_i). The equation of motion includes the pressure gradient, electron friction, and electromagnetic forces,

$$m_i\frac{du_i}{dt} = -\frac{\nabla p_i}{n_i} + (u - u_i)\nu_m + Ze(E + u_i\times B). \tag{6}$$

The new modeling pertaining to the intense interaction of the heavy ion beam with the discharge plasma, first discussed in Ref. 23, is now described. Plasma electron densities are advanced with the following equation:

$$\frac{\partial n_e}{\partial t} = \nabla\cdot J_e + w^{-1}\frac{dE}{dt}f_bn_b, \tag{7}$$

where dE/dt is the fraction of the Bethe collisional energy-loss rate of the beam ions from interaction with the bound Xe electrons. For simplicity, we assume this fraction f_b is the ratio of bound electrons to the Xe atomic number. The energy to produce an ionization, $w = 25$ eV for neutral Xe,[26] is assumed to increase with the square of the new ionization state. Due to the expected high electron temperatures and dominant effect of ion impact ionization, we neglect the effects of electron recombination and avalanche in these calculations. Energy-dependent electron-neutral momentum transfer frequencies[26] and Spitzer collision frequencies for the electron-ion interaction are used with anomalous resistivity ignored.

The extremely rapid evolution of the electron energy and the multiple stripping of the Xe atoms demand a more detailed model. Thus, the electron energy equation has been modified to account for time-dependent evolution unlike the usual steady-state approximation in which all electron attributes are modeled as a function of the ratio of electric field-to-ambient gas density (E/p). In the new model, the evolution of T_e is described by the equation,

$$\frac{3}{2}n_e\frac{dT_e}{dt} = \frac{3n_em_e}{m_i}\frac{(T_i - T_e)}{\tau_{ie}} + 1.96n_ev_e^2\nu_m + \nabla\cdot\kappa\nabla T_e + Q_e, \tag{8}$$

where T_i and v_e are the ion temperature and the electron velocity. The first term on the right-hand side (RHS) of Eq. (8) is the ion-electron thermalization. The next term is the Ohmic heating term. The thermal diffusion term (third term on the RHS of the above equation) is characterized by the thermal conductivity κ. The ion-beam heating term Q_e assumes that a fraction $(1 - f_b)$ of the Bethe energy loss for neutral Xe is deposited in the free electrons. Thus, we ignore the weak effects of the multiply charged gas (which only show up in the Coulomb logarithm). Inelastic losses of free electrons, such as radiation and excitation of bound electrons, are neglected.

Several approximations are also made concerning the beam interaction with the plasma. Described in Ref. 24, we assume the Moliere multiple-scattering formalism and Bethe slowing down in neutral Xe. Finally, the beam charge state is held fixed and is assumed to have stripped to this state (e.g., Pb^{+72}) in the ballistic drift section before entering the adiabatic discharge section. A modest spread in charge state, from examination of Eq. (4), would not have significant impact on the final radius.

The IPROP code is used to simulate the intense beam interaction with a Xe plasma for APT in an HIF chamber. We use a realistic set of ''foot'' and ''main'' pulses that are required to couple into the hybrid target design of Callahan and Tabak.[27] This hybrid target requires a larger beam spot of roughly 5 mm relative to the distributed radiator target (3-mm spot).[28] The foot beam is a lower energy and current beam that preheats the hohlraum. The main pulse arrives immediately after the foot pulse and drives the radiation temperature in the hohlraum to its peak value. In our simulations, the foot pulse is a 12.5-kA (particle current), 3-GeV, and 25-ns pulse length Pb^{+72} ion beam. The main pulse has a 66.5-kA current, 4.5-GeV energy, and 8-ns pulse length. These uniform density beams are injected with a 30-cm outer radius, 10 m upstream from the discharge. The microdivergence (θ_i = rms deviation of the mean transverse beam motion) is taken as 1 mrad. The beam is transported ballistically over a distance of 10 m reaching roughly an 8-mm outer radius (r_s) at the entrance to the discharge.

The adiabatic discharge channel has an axially dependent radius and reduced density (falling linearly from 5 Torr at $z = 0$ to 0.5-Torr for $z > 125$). The discharge is sharp-edged with $r_{ci} = 2$ cm falling linearly to $r_{cf} = 0.5$ cm at $z = 125$ cm (distance from the entrance to the adiabatic discharge channel). The Xe ionization fraction is initially 0.9 with a 3-eV plasma temperature. The current density, reduced gas density, and the ionization fraction have square radial profiles. The initial conductivity is 3.9×10^{13} s^{-1} within the channel.

In our nominal simulation, we examine a 50-kA discharge in which the simple theory (see Sec. II) predicts the beam edges should compress to roughly 4.6 mm. The beam particles at various propagation times through the discharge

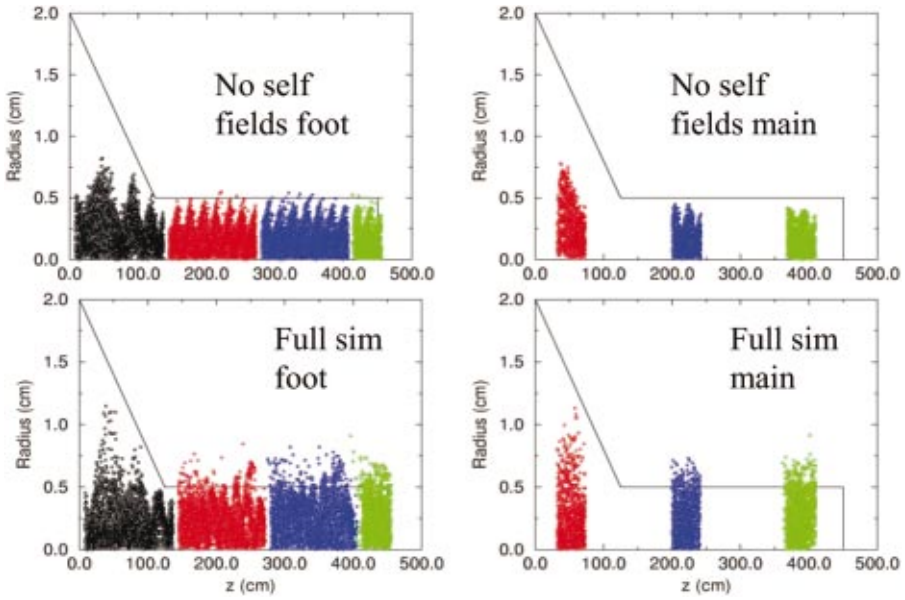

FIG. 2. (Color) The positions of the foot (left) and main (right) pulse beams are shown after 27, 54, 80, and 97 ns. The two upper figures are IPROP simulation results with no self fields and the two lower figures are the full simulation results.

are shown in Fig. 2 for IPROP simulations without and with self fields. As expected, without self fields the beam is compressed in the adiabatic lens section to an outer radius of roughly 4.5 mm. With self fields, however, as the beam oscillations slowly damp, a low-density halo of beam ions forms. The local growth of self fields is very sensitive to the plasma electron temperature evolution that sets the plasma resistivity through Spitzer. T_e rises on-axis to nearly 4 keV at the beam waists. Within 2 ns at a given z position, the temperature rise increases the conductivity above 10^{15} s^{-1} and rises to nearly 10^{16} s^{-1} after 20 ns (near the back of the foot pulse). The average charge state of the Xe gas rises to 10–15 by this time and plateaus. The plasma monopole magnetic decay time also increases to nearly 5 μs, sufficiently long to slow self-field growth as described in the previous section. The spatial variation of the magnetic fields after 80 ns is plotted in Fig. 3. We see significant axial rippling of the self field that reaches a maximum of 45 kG. The total net current, calculated at the radius containing half the beam current, increased to only 80 kA. The net current growth is of the order of that predicted at the end of Sec. II for magnetic diffusion. Inhibition of the plasma return current from magnetic tensor effects does not significantly enhance net current growth. As a result, inductive energy losses are tolerable (roughly 4%). This loss is less than the 6% loss due to collisional interactions with the gas. A plot of the time-integrated beam deposition for this simulation compared with an ideal simulation, where no scattering or self fields are modeled, is shown in Fig. 4. The time-integrated beam rms radius on target is 3.5 mm. The total energy transport efficiency at 450 cm is 85%. The main deleterious effect of the propagation is the formation of a halo. Some ions interact with the oscillating self-magnetic field imprinted by the gross beam motion shown in Fig. 3. These ions are kicked out to larger radius where they scatter in the more dense 5-Torr wings. The core of the beam remains focused.

We now look for any sensitivity in the beam transport as the channel current and beam divergence is varied. The stability of the discharge channel can be a function of the discharge current; a reduction of this current is preferable. IPROP simulations of discharge currents from 25–75 kA were run. The sensitivity of the transported beam energy was quite small. As the current dropped from 75 kA to 25 kA, the efficiency of transported beam energy within 5 mm fell from

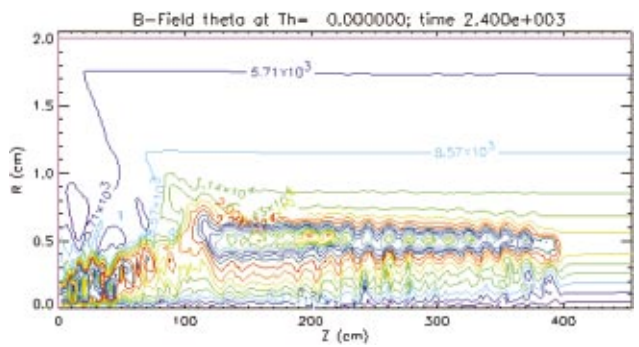

FIG. 3. (Color) Contours of the magnetic fields at 80 ns (beam head is at $z=408$ cm) for the nominal IPROP with self fields is plotted. In this case, the Pb^{+72} ion beam is injected into a 50-kA discharge channel.

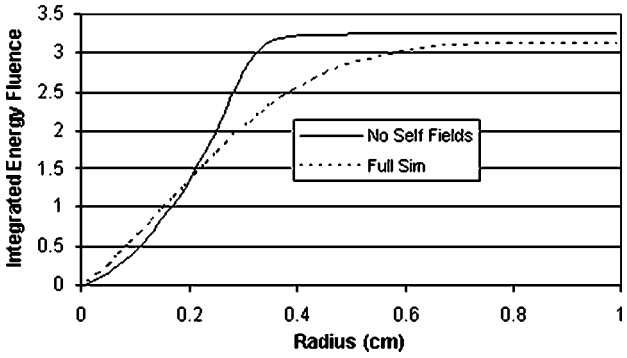

FIG. 4. The time-integrated beam energy deposition at the target ($z=450$ cm) is plotted for the nominal beam/channel simulations. The energy has been radially integrated to yield the beam energy contained within a given radius.

87% to 80%. At 25 kA, the beam profile was becoming more annular and a more rapid loss of efficiency is expected for lower discharge currents. Similar results were found as the beam divergence is increased from 1 to 2 mrad. The transport efficiency falls from 85% for 1 mrad to 81% for 2 mrad. Again, at the higher divergence value, the profile beam becomes more annular.

We also expect little variation in beam transport efficiency for different beam ions. If we assume a fixed beam charge-state fraction of the atomic number, the charge-to-mass ratio of the ion is nearly constant and their confinement in the electromagnetic fields of the channel is also nearly a constant. Furthermore, the ion velocity of $0.2c$ determines the optimal range in the target radiator. Thus, in order to keep the energy on target fixed, as the ion mass decreases, the ion energy decreases in proportion and the total ion current must increase. The electrical current is then also nearly a constant. The only major difference in the beam/gas interaction is the beam impact ionization and the beam energy loss in the gas, which are, of course, related. Using IPROP, we simulate a Xe^{+44} beam keeping the total beam energy fixed. The resulting transported beam energy within 5 mm was identical to the Pb beam at 85% although the radial profiles were not identical. These results show little sensitivity to fairly large variations in discharge or beam conditions.

IV. SEMIANALYTIC RESISTIVE HOSE THEORY

As with any propagating beam in a resistive medium, particularly given a strong plasma return current, APT is susceptible to the dipole ($m=1$) "hose" instability. Hose is a resistive instability driven by the phase lag between the perturbed beam current and the plasma return current. Closed expressions for the growth time of the instability have been derived for Bennett beam and conductivity radial profiles with half-current radius r_b. Ignoring plasma current neutralization, the e-folding time for the fastest growing mode in the beam frame is given by $0.69\tau_d$,[29] where the dipole decay time $\tau_d=\pi\sigma r_b^2/2c^2$. Lampe[30] found the e-folding time in the highly current neutralized limit is $\tau_e\sim 0.59\tau_d I_{\rm net}/I_b$. τ_e increases with $I_{\rm net}$, suggesting higher current discharges are preferable. Note that the net current growth and characteristic hose growth time have the same σr_b^2 scaling. We expect a strong coupling between the equilibrium and dipole behavior.

To study the complex interaction between net current evolution and hose growth, we used IPROP, adding a second azimuthal mode ($m=1$). This work was presented in an earlier paper.[23] In these simulations, the conductivity was not permitted to evolve and only pinched propagation with constant channel radius of 0.5 cm was modeled (the simulations did not include the adiabatic lens section). The hose growth over 2-m propagation was seen to be benign. In some cases, with conductivity consistent with that calculated in the above 2D simulations (with 2-μs dipole decay length), beam perturbations simply damped. As the conductivity was reduced yielding an 80-ns decay length, the beam centroid grew only a factor of 2, much less than simple theory suggested. In this section, we present detailed analytic modeling that suggests betatron detuning as the explanation for the enhanced stability of the beam-to-hose motion.

We make use of the well-known spread-mass model introduced by Lee[29] to include orbital phase-mixing effects into the analysis of the resistive hose instability. For a Bennett beam of radius r_b and current I_b, and a fixed conductivity profile $\sigma(r)$ with on-axis peak value σ_o, the spread-mass equations may be written as

$$\frac{\partial^2 Y_\eta}{\partial z^2}=-\eta k_\beta^2\left\{Y_\eta-\frac{1}{1-f}\int_0^\infty\frac{6u^2r_b^4cA_1(u)}{(u^2+r_b^2)^3I_b}du\right\}, \tag{9}$$

$$\frac{\partial}{\partial r}\left\{\frac{1}{r}\frac{\partial}{\partial r}[rA_1(r)]\right\}-\frac{8\tau_B\sigma(r)}{r_b^2\sigma_0}\frac{\partial A_1}{\partial\tau}=-\frac{16rr_b^2I_b}{(r^2+r_b^2)^3c}\langle Y_\eta\rangle, \tag{10}$$

where $\tau=t-z/v_z$ measures time back from the head of the beam,

$$k_\beta^2=\frac{2q\beta I_b(1-f)}{\gamma Mcv_z^2r_b^2}, \tag{11}$$

$$\tau_B=\frac{\pi\sigma_0r_b^2}{2c^2}, \tag{12}$$

is the dipole decay time, and f is the neutralization fraction $[I_{\rm net}=(1-f)I_b]$. In Eqs. (9) and (10), Y_η is the centroid of the beam disk labeled by the index η $(0\leqslant\eta\leqslant 1)$ and $A_1(r)$ is the perturbed magnetic vector potential. The angle brackets denote the mean value of a quantity, e.g.,

$$\langle Y_\eta\rangle=\int_0^1 d\eta g(\eta)Y_\eta, \tag{13}$$

where $g(\eta)=6\eta(1-\eta)$ is the weighting function for a Bennett beam. For perturbations of the usual form $\exp(i(\omega\tau+kz))$, where k denotes the Doppler-shifted wave number, the equations may be combined to give

$$\frac{\partial}{\partial r}\left\{\frac{1}{r}\frac{\partial}{\partial r}[rA_1(r)]\right\}-\frac{8i\omega\tau_B\sigma(r)A_1(r)}{\sigma_0r_b^2}=-\frac{24rr_b^6}{(r^2+r_b^2)^3(1-f)}\left\langle\frac{\eta k_\beta^2}{\eta k_\beta^2-k^2}\right\rangle\int_0^\infty\frac{4u^2A_1(u)du}{(u^2+r_b^2)^3}. \tag{14}$$

For the special case of a Bennett conductivity profile with channel radius r_c equal to the beam radius r_b, Lee[29] showed that Eq. (14) implies

$$A_1(r)\propto\frac{rr_b}{(r^2+r_b^2)}, \tag{15}$$

which leads to the dispersion relation

$$\omega_i\cong\frac{(f+0.69)}{(1-f)\tau_B}. \tag{16}$$

Maximizing $\mathrm{Im}(-\omega)$ for real k gives a peak temporal growth rate[29,30] of

TABLE I. Results from numerical integration of Eqs. (9) and (10) for various values of net current and beam radius. (Flat conductivity profile with $\sigma_0 = 2\times 10^{14}\ s^{-1}$.)

r_b (cm)	I_{net} (kA)	k_β (cm^{-1})	τ_B (ns)	e-foldings
0.500	50	0.147	87.0	3.88
0.354	100	0.294	43.5	3.76
0.289	150	0.441	29.0	3.67
0.250	200	0.588	21.8	3.60
0.224	250	0.735	17.4	3.53
0.204	300	0.882	14.5	3.47

$$i\omega\tau_B = \frac{f + \left\langle \frac{k^2}{\eta k_\beta^2 - k^2} \right\rangle}{(1-f)} \tag{17}$$

for $k \cong 0.52\, k\beta$.

In order to consider the implications of arbitrary conductivity profiles, we discretize Eq. (14) by setting $r = n\Delta r$, $n = 1,2,3,...$ to obtain an infinite system of linear equations for the components of the vector $A_1(n\Delta r)$. The system may be truncated at some large $n\Delta r$ (typically 20 to 30 r_b in these calculations), and the determinant of the resulting coefficient matrix set equal to zero to obtain a dispersion equation. Keeping the Bennett shape for convenience, we find

$$\omega_i \cong \frac{(f+0.69)}{(1-f)\tau_B} h\left(\frac{r_c}{r_b}\right), \tag{18}$$

where r_c is the (Bennett) radius of the conductivity profile. Some values of h determined by the numerical procedure outlined above are $h(1)=1$, $h(2)=0.413$, $h(4)=0.318$, $h(\infty)=0.292$, the last value corresponding to the flat conductivity profile case. For beams nearly fully neutralized, f is near 1, and we see immediately from Eq. (17) that the peak temporal growth rate scales approximately as

$$\omega_i \propto \frac{1}{I_{net} r_b^2}. \tag{19}$$

For the present case (4 GeV Pb^{+72} ion beam), it was observed in the simulations[23] that the net current and beam radius varied from 50 kA and 0.5 cm at the beam head to approximately 300 kA and 0.204 cm at the tail. For a nearly flat conductivity profile, these values, according to Eq. (19), give a constant ''local'' growth rate along the beam. Using Eq. (18) with $\sigma_0 = 2\times 10^{14}\ s^{-1}$ and again a flat conductivity profile gives an asymptotic upper bound on the growth at the tail of an 8-ns beam of about 5.2–5.7 e-foldings (depending on exactly which point along the beam is chosen to define I_{net} and r_b). Direct numerical integration of the coupled differential Eqs. (9) and (10) was also carried out to determine expected growth at the end of the 8-ns pulse. Results from six such integrations are shown in Table I, with the predicted number of e-foldings in the last column. For each case, the value of $I_{net} r_b^2$ is the same, and we see that the growth varied only slightly (over the range 3.5–3.9 e-foldings), consistent with the scaling inferred from the dispersion analysis above.

Although the ''local'' growth rate remains approximately constant along the beam, the spatial (betatron) wave number at peak growth ($k \cong 0.52\, k_\beta$) varies as $I_{net}^{1/2}/r_b$, corresponding to wavelengths of 22.2 cm at the beam head to 3.7 cm at the tail. These values are in good agreement with those inferred from the IPROP simulations of Ref. 23. Accordingly, Eqs. (9) and (10) were again integrated numerically, this time with I_{net} and r_b varying with τ during the course of the integration from 50 kA and 0.5 cm at the beam head ($\tau = 0$) to 300 kA and 0.204 cm at the tail ($\tau = 8$ ns). The result of this calculation was approximately 1.3 e-foldings of growth, substantially less than the constant net current and beam radius cases summarized in Table I. This lends strong support to the notion that the variable betatron wavelength (betatron detuning) is the explanation for the relatively low hose growth observed in the simulations.

V. CONCLUSIONS

Using semianalytic theory and the IPROP code, we have examined the APT mode currently under consideration for HIF chamber transport. The key advantage of the pinched modes is that the beams are focused before the chamber. Thus, the focal length of the beam is separable from the transport length in the chamber. This separation potentially relaxes the accelerator requirements on emittance. The APT simulations are encouraging in that nearly 90% energy transport is achieved. The plasma conductivity mitigates both $m = 0$ net current growth and $m = 1$ hose instability growth. We find that even for conductivity well below that calculated by IPROP, the hose motion is effectively reduced due to the rapidly changing beam betatron wavelength that detunes the instability. The wavelength increases rapidly as self-magnetic fields grow in the resistive medium. This observation, first seen in simulations, is confirmed in a spread-mass analytic model of the resistive hose including variable current neutralization effects. This model shows that the hose growth for a beam with wavelength decreasing in time is less than for a beam that had a constant small wavelength. This work suggests that APT is a robust chamber transport scheme worthy of continued consideration for HIF.

ACKNOWLEDGMENTS

We express our appreciation for useful discussions and support to Grant Logan, Alex Friedman, William Sharp, Christine Celata, Ron Davidson, and the ARIES Team. Work supported by ARIES, the Virtual National Laboratory for Heavy Ion Fusion, the Department of Energy through Princeton Plasma Physics Laboratory, and Lawrence Berkeley National Laboratory.

[1] R. O. Bangerter, Nucl. Instrum. Methods Phys. Res. A **415**, 3 (1998).
[2] C. L. Olson, J. Fusion Energy **1**, 309 (1982).
[3] B. G. Logan and D. A. Callahan, Nucl. Instrum. Methods Phys. Res. A **415**, 468 (1998).
[4] S. Yu, S. Eylon, T. Fessenden, E. Henestroza, R. Lafever, W. Leemans, R. Petzoldt, D. Ponce, M. Vella, R. W. Moir, W. M. Sharp, R. Peterson, M. Sawan, and A. Tauschwitz, Nucl. Instrum. Methods Phys. Res. A **415**, 174 (1998).
[5] J. N. Olsen and R. J. Leeper, J. Appl. Phys. **53**, 3397 (1982).
[6] T. Ozaki, S. Miyamota, K. Imasaki, S. Nakai, and C. Yamanaka, J. Appl. Phys. **58**, 2145 (1985).
[7] D. R. Welch and C. L. Olson, Fusion Eng. Des. **32–33**, 477 (1996).

[8]P. F. Ottinger, D. V. Rose, and B. V. Oliver, Phys. Plasmas **6**, 3717 (1999).
[9]D. V. Rose, P. F. Ottinger, D. R. Welch, B. V. Oliver, and C. L. Olson, Phys. Plasmas **6**, 4094 (1999).
[10]P. F. Ottinger, F. C. Young, S. J. Stephanakis, D. V. Rose, J. M. Neri, B. V. Weber, M. C. Myers, D. D. Hinshelwood, D. Mosher, C. L. Olson, and D. R. Welch, Phys. Plasmas **7**, 346 (2000).
[11]C. L. Olson, Nucl. Instrum. Methods Phys. Res. A **464**, 118 (2001).
[12]D. A. Callahan, Fusion Eng. Des. **32–33**, 441 (1996).
[13]R. W. Moir, Nucl. Instrum. Methods Phys. Res. A **464**, 140 (2001).
[14]W. M. Sharp, D. A. Callahan-Miller, A. B. Langdon, M. S. Armel, and J.-L. Vay, Nucl. Instrum. Methods Phys. Res. A **464**, 284 (2001).
[15]J. M. Neri, P. F. Ottinger, D. V. Rose, P. J. Goodrich, D. D. Hinshelwood, D. Mosher, S. J. Stephanakis, and F. C. Young, Phys. Fluids B **5**, 176 (1993).
[16]J. N. Olsen and L. Baker, J. Appl. Phys. **52**, 3286 (1981).
[17]D. M. Ponce, C. Niemann, S. S. Yu, W. P. Leemans, T. J. Fessenden, G. Dahlbacka, W. M. Sharp, and A. Tauschwitz, Nucl. Instrum. Methods Phys. Res. A **464**, 331 (2001).
[18]E. Boggasch, A. Tauschwitz, H. Wahl, K.-G. Dietrich, D. H. H. Hoffmann, W. Laux, M. Stetter, and R. Tkotz, Appl. Phys. Lett. **60**, 2475 (1992).
[19]A. Tauschwitz, S. S. Yu, S. Eylon, R. O. Bangerter, W. Leemans, C. Peters, J. O. Rasmussen, L. Reginato, J. J. Barnard, and W. M. Sharp, Fusion Eng. Des. **32–33**, 493 (1996).
[20]P. F. Ottinger, D. Mosher, and S. A. Goldstein, Phys. Fluids **23**, 909 (1980).
[21]J. J. Watrous, P. F. Ottinger, and D. Mosher, Phys. Fluids B **2**, 378 (1990).
[22]J. M. Neri, J. R. Boller, F. C. Young, G. Cooperstein, D. D. Hinshelwood, D. Mosher, P. F. Ottinger, V. E. Scherrer, S. J. Stephanakis, and J. J. Watrous, in *Proceedings of the Seventh International Conference on High-Power Particle Beams*, edited by W. Bauer and W. Schmidt, Karlsruhe, Germany, 4–8 July 1988, ISBN 3-923704-01-1 (Kernforschungszentrum Karlsruhe GmbH Literaturabteilung, Germany, 1988), p. 165.
[23]D. R. Welch, D. V. Rose, B. V. Oliver, T. C. Genoni, R. E. Clark, C. L. Olson, and S. S. Yu, Phys. Plasmas **9**, 2344 (2002).
[24]D. R. Welch, C. L. Olson, and T. W. L. Sanford, Phys. Plasmas **1**, 764 (1994).
[25]E. Henestroza, S. Yu, M. C. Vella, and W. M. Sharp, Nucl. Instrum. Methods Phys. Res. A **415**, 186 (1998).
[26]L. G. H. Huxley and R. W. Crompton, *The Diffusion and Drift of Electrons in Gases* (Wiley, New York, 1974).
[27]D. A. Callahan, M. C. Herrmann, and M. Tabak, Laser and Particle Beams (to be published).
[28]D. A. Callahan-Miller and M. Tabak, Nucl. Fusion **39**, 883 (1999).
[29]E. P. Lee, Phys. Fluids **21**, 1327 (1978).
[30]M. Lampe, W. Sharp, R. F. Hubbard, E. P. Lee, and R. J. Briggs, Phys. Fluids **27**, 2921 (1984).